Int. j. adv. multidisc. res. stud. 2026; 6(6):854-863

Received: 30-09-2026
Accepted: 10-11-2026

International Journal of Advanced Multidisciplinary Research and Studies

ISSN: 2583-049X

From Selected Peak Heights to Spatial Diffraction Maps in Semiconductor Crystals

Konstantinos T Kotsis
Lab of Physics Education and Teaching, Department of Primary Education, University of Ioannina, Greece

DOI: https://doi.org/10.62225/2583049X.2026.6.6.7194
Corresponding Author: **Konstantinos T Kotsis**

Abstract
Spatial contrast in X-ray diffraction does not uniquely determine the crystalline property represented by a map. This critical methodological synthesis examines the information lost when spatially sampled diffraction profiles are reduced to selected peak maxima and specifies the additional measurements needed for defensible structural inference. A documented Ge(111) translation series from a 1986 doctoral dissertation provides eleven experimental peak-height observations, with additional-to-reference ratios from 0.07313 to 0.34110. Two explicitly hypothetical Gaussian profile families reproduce all eleven ratios yet yield either spatially varying integrated angular area at fixed width or constant area with varying width. The resulting widths (10.07–46.97 arcsec) are mathematical constructions, not recovered measurements. A separate line-to-surface counterexample establishes that a single spatial transect cannot determine transverse contrast. The analysis distinguishes real-space localization, reciprocal-space coverage, instrumental response and structural identifiability; it compares rocking-curve imaging, reciprocal-space mapping, scanning microdiffraction, dark-field microscopy and coherent Bragg methods. Its specific contribution is a claim-conditioned measurement workflow that identifies the evidence required to advance from an operational map of intensity descriptors to interpretations such as strain or defect population. The workflow is proposed, not experimentally validated; no new diffraction maps or recovered historical profiles are reported.

Keywords: X-ray Diffraction, Semiconductor Characterization, Rocking-curve Imaging, Reciprocal-space Mapping, Peak-Height Analysis

1. Introduction

A diffraction image becomes a structural measurement only through an account of what its intensity represents. Variations across a crystal can arise from changes in diffracting volume, local orientation, lattice distortion, diffuse scattering, illumination, or angular acceptance. Several of these effects can coexist within one image. A map that is highly reproducible as an intensity distribution may therefore remain ambiguous as a map of strain, surface damage, or defect concentration.

This problem is present even in comparatively simple spatial scans. Moving a crystal through a narrow beam can reveal differences between selected diffraction features. Such observations establish that the measured response changes with position. The further interpretation depends on which angular information was retained, how the illuminated region was defined, and what physical model connects the signal to the intended measurand. Increasing the number of spatial samples does not automatically supply information discarded when a profile is reduced to one peak height.

The historical context examined here is research on scattering near a reciprocal-lattice point. [1] Proposed topographic use of an additional diffraction component associated with surface imperfections. [2] investigated the influence of crystal asymmetry on near-Bragg diffraction patterns. The doctoral thesis of [3] includes a spatial translation experiment in which the additional peak changes relative to two dynamical features. These studies provide a documented starting point for asking how selected-component contrast could be developed into spatially resolved characterization under more explicit measurement conditions.

Modern methods supply several ways to retain more information. Reciprocal-space mapping resolves the angular distribution around a reflection [4]. Rocking-curve imaging associates spatially registered images with an angular scan, allowing profile descriptors to be extracted at each image location [5]. Recent work on 4H-SiC illustrates the value of treating complex profiles beyond a simple maximum and a single fitted width [6]. These developments do not reconstruct the information absent from an archival peak table, but they clarify the measurements that would address its ambiguities.

Other approaches interrogate different aspects of crystalline structure. Scanning microdiffraction can combine spatial localization with orientation and strain information under a specified diffraction geometry [7]. Dark-field X-ray microscopy uses diffracted-beam imaging optics to examine selected internal volumes [8]. Coherent diffraction and Bragg ptychography introduce reconstruction methods that recover information from measured diffraction distributions under additional coherence and modelling requirements [9, 10]. These techniques are considered here as different routes from observations to structural claims, rather than as a simple sequence in which one method replaces every earlier method.

The article addresses what is gained when peak summaries become spatially registered angular datasets, what remains ambiguous, and which measurements are necessary for stronger structural interpretation. Its contribution combines a critical narrative synthesis with a constructive demonstration of non-uniqueness. The archival data anchor the argument, while hypothetical profiles are used only to show what the retained peak heights do not determine. The study reports no newly measured map and does not present the historical topographic principle as a new discovery.

The methodological gap addressed here is not whether peak height differs from integrated intensity, which is elementary, but how that loss of information should govern claims made from a spatial diffraction dataset. The work therefore asks three questions: (i) which distinct angular distributions are observationally indistinguishable after peak-height reduction; (ii) which spatial and instrumental ambiguities remain after an angular descriptor is mapped; and (iii) which minimum additional measurements permit an investigator to move from a map of operational observables to a claim about crystalline structure. The original contribution is a claim-conditioned evidence framework, illustrated using documented archival contrast, rather than a new inversion theorem or a newly invented diffraction-imaging technique.

2. Theoretical Background

A spatial diffraction measurement has both a real-space coordinate and a scattering coordinate. The former identifies where the specimen is sampled; the latter identifies the angular or reciprocal-space region accepted by the instrument. A conventional intensity image records a selected combination of these coordinates. A rocking-curve image stack retains an angular dependence at each registered location. A reciprocal-space map retains intensity over a defined region of scattering-vector space. Neither the word image nor the word map specifies the structural interpretation without these coordinate definitions.

For a resolved component with background removed, let P(r,ω) denote the measured angular profile at specimen position r. Its maximum H(r), angular position μ(r), width w(r), and area A(r) are different descriptors. The maximum is the largest recorded value within a specified angular interval. The area integrates the profile over an interval that must also be specified. Width depends on a chosen definition and may be ambiguous for overlapping or split peaks. A peak position need not equal a centroid, especially for asymmetric profiles. These differences become consequential when a map uses one descriptor as a proxy for another.

A Gaussian profile offers a simple illustration of the information involved.

$$P(r,\omega) = H(r)\, exp[-4\, ln(2)\, \frac{(\omega - \mu(r))^2}{w(r)^2}]$$

Here w is the full width at half maximum. If the integration interval contains the entire ideal Gaussian, its area is given by the following expression.

$$A(r) = H(r)\, w(r) \sqrt{\frac{\pi}{4\, ln(2)}}$$

Consequently, the height alone cannot determine the area unless the width and profile form are constrained. The Gaussian assumption is used below as an analytical counterexample. It is not proposed as a universal model of dynamical diffraction, an experimental fit, or a deconvolution of the archived measurements.

The same non-identifiability is not specific to the Gaussian function. Consider any non-negative integrable shape f with f(0) = 1 and finite integral C = ∫f(t)dt. A family P(ω; x) = h(x)f((ω − μ(x))/s(x)) has maximum h(x), provided f has unit maximum, while its area is A(x) = C h(x)s(x). Thus a fixed scale s yields an area proportional to h, whereas choosing s(x) proportional to 1/h(x) yields constant area. This scale-family argument applies to numerous symmetric or asymmetric admissible illustrative profiles; it does not establish that every such profile is physically realizable in a particular dynamical diffraction geometry. Physical response constraints, instrumental convolution, truncation and overlap can restrict the permissible families, but measured maxima alone do not supply those restrictions.

A fixed-angle image differs from a map of tracked maxima. If a narrow profile shifts while retaining its shape and area, its intensity at one fixed angular setting can change considerably. By contrast, the true maximum of the same profile remains constant if the full peak is sampled and tracked. A height map may still change through broadening, redistribution between overlapping components, or variation in the total selected-channel intensity. These mechanisms should not be conflated. Incomplete scan coverage can introduce further ambiguity by failing to include the displaced maximum.

The apparatus modifies the observed profile. Dynamical theory describes coherent wave coupling in nearly perfect crystals [11], while the source, monochromator, analyser, and acceptance contribute to the recorded angular response [12]. Explicitly examine the resolution function of a triple-crystal diffractometer. A measured width therefore cannot be assigned wholly to the specimen without a justified response calculation or calibration. [13] Provide a computational implementation for perfect-crystal diffraction that can inform modelling of crystal optics, but a specimen with deformation or surface disorder requires additional physical description.

Spatial localization introduces another response. A phenomenological intensity-averaging description may be written as follows.

$$I_j(r,\omega) = \int_{\Omega} W_j(r,r')\, S_j(r',\omega)\, d^2r' + B_j(r,\omega)$$

The kernel W_j describes spatial sensitivity for component j, Ω is the contributing specimen region, and B_j is an additive contribution. This expression is useful when the measurement can be treated as an incoherent or effectively averaged local response. It is not a general replacement for

coherent amplitude propagation. Near an edge, the contributing region changes, and two components need not have identical kernels. A ratio of two spatial integrals is not generally the local ratio of their underlying specimen responses.

The spatial sampling increment Δx, illumination footprint and demonstrated resolving power must not be identified with one another. An increment is a coordinate spacing; a footprint is a sensitivity distribution, potentially dependent on incidence angle and specimen boundaries; spatial resolution is an experimentally supported ability to distinguish separated specimen features under the measurement operator. Translating in steps smaller than the footprint can oversample essentially the same region, whereas large steps may miss localized variation. The effective kernel should be characterized separately for each selected component when their angular acceptance or penetration differs.

Structural interpretation also depends on reciprocal-space geometry. For a small deformation, the change in a reciprocal-lattice vector can contain both strain and rotation contributions. In one linearized convention, $\Delta G \approx -\varepsilon^{T}G + \Omega_{r}G$, where ε is the symmetric strain tensor and Ω_r is the antisymmetric infinitesimal rotation tensor. A single measured angular displacement does not independently determine both. Multiple non-equivalent reflections or other constraints are needed for a fuller tensor interpretation. The familiar relation between lattice spacing and Bragg angle applies only after the relevant geometrical and orientation effects have been separated.

Surface-related contrast is similarly non-unique. Crystal termination produces reciprocal-space intensity away from ideal lattice points, while roughness modifies scattering under specified statistical and optical assumptions [14, 15]. [16] describe diffraction from crystals with defined surface relief within dynamical theory. These contributions show why an increased or decreased selected peak cannot uniquely specify a defect concentration. The historically used label kinematical identifies a component in the source analysis; it is not treated here as a complete microscopic assignment.

A quantitative map must therefore define its measurand. A map of peak height, angular position, width, or integrated intensity can be operationally meaningful even before a unique structural mechanism is established. A map of defect density or a strain tensor requires a further calibrated relationship between measured observables and those quantities. The distinction concerns the evidence supporting the interpretation, rather than the visual quality or spatial density of the displayed image.

3. Method

The study combines a critical narrative synthesis with a worked archival example and analytical constructions. Literature was selected purposively to cover the information supplied by angularly resolved diffraction, spatially resolved measurements, surface-sensitive scattering, and coherent reconstruction. Searches of scholarly web records and publisher resources were updated on October 29, 2026, using combinations of rocking-curve imaging, reciprocal-space mapping, semiconductor diffraction, peak shape, surface scattering, spatial resolution, and Bragg ptychography. Foundational work was retained alongside recent studies when it established a physical distinction needed for the argument. The review is not systematic, does not estimate the prevalence of a result across all semiconductor materials, and does not claim that the selected methods exhaust available characterization techniques.

To make the purposive selection auditable without representing it as a systematic search, the sources were grouped by their role in the argument: Foundational diffraction and instrumental response; angular-profile and reciprocal-space measurements; spatially localized imaging; coherent reconstruction; and semiconductor-specific applications. Inclusion was based on whether a study clarified a distinct measurement operator, a known ambiguity, or a practical means of adding an independent constraint. Work on metals or non-semiconductor crystals was retained only for transferable measurement principles, not as evidence that the same quantitative performance holds in Ge. No exhaustive database coverage, prespecified screening flow, or pooled performance estimate is claimed; the records of searches and counts needed for those claims were not available in the source material.

The synthesis compared the methods according to the measured data, the derived observables, and the assumptions required for structural interpretation. Studies of metallic or optical crystals were included where they demonstrate a measurement principle, with their material context identified. Semiconductor examples were used to establish direct relevance to the intended characterization problem. Reported resolutions and sensitivities were not pooled because they refer to different geometries, specimens, and definitions. No numerical performance ranking is inferred from these heterogeneous studies.

The archival source is the supplied doctoral dissertation of [3]. The citation follows the date on its title page; the repository catalogue assigns 1987. Table VII on printed page 200, corresponding to page 211 of the supplied PDF, contains eleven Ge(111) observations at positions separated by 2 mm. The accompanying discussion on printed pages 201–202 explains the comparison of the components and identifies a restricted interior interval. The present study uses the complete table to examine what its retained representation can determine. The associated 1985 and 1986 journal papers provide historical context, rather than independent replications of this spatial series.

The archival series was chosen because it reports three component-specific rates at identical listed translation coordinates, so both the available contrast and the information discarded by the tabulation can be identified precisely. It is not a random or representative sample of semiconductor specimens. The original tabulation documents a detuning of 70 arcsec, but the materials available for this analysis do not provide a recoverable position-dependent beam-footprint function, complete raw scans, background model, or uncertainty budget. Accordingly, no spatial resolution, strain field, penetration-depth distribution, or defect density is inferred from the 2 mm position increment or from the K/R ratio.

The table reports peak rates for an additional component K, a residual dynamical component R, and a virtual dynamical component V at a reported specimen detuning of 70 arcsec. Entries were checked visually against the scanned table and retained at the published decimal precision. The derived quantity $h(x) = K(x)/R(x)$ is a ratio of peak heights. It is not an incident-flux-normalized cross section, an integrated intensity ratio, or a pointwise defect density. Its role in the

analytical example is to provide eleven documented maxima to which alternative angular profiles can be matched.

The normalization h = K/R is operational: K and R are different diffraction components, and equality of their incident-flux dependence or spatial sensitivity cannot be assumed merely because their maxima were recorded at the same nominal location. A stable V/R ratio can offer an internal contrast comparison, but does not prove that illumination, acceptance, or boundary effects cancel in K/R. In the absence of independently measured component-specific kernels and an acquisition response model, h should be described strictly as relative peak-height contrast.

Two Gaussian families were constructed from these ratios. In the first family, all widths equal an illustrative $w_0 = 20$ arcsec and each maximum equals the corresponding h(x). In the second family, the width is $w_2(x) = w_0 h(10\ \text{mm})/h(x)$. Both families use an arbitrary common centre $\mu = 0$ solely to define the illustration. Their analytic integrals were calculated using the Gaussian area relation. The second construction has exactly constant area because the product $h(x)w_2(x)$ is fixed. Neither width family nor its common centre was measured, inferred as the actual line shape, or fitted to raw profiles. No realistic dynamical response is implied by their numerical proximity to any historical width.

The construction tests whether peak heights uniquely determine angularly integrated intensity. One pair of distinct admissible mathematical profile families with identical maxima is sufficient to demonstrate that they do not, in the absence of additional profile constraints. The calculation does not compare the likelihood of those families, reconstruct the true historical angular distribution, or establish which physical process produced the archived contrast. Its units follow the illustrative integral over angle: h is dimensionless and its angular integral is expressed in arcseconds.

A second construction addresses the real-space dimensionality of the record. Let g(x) be a positive smooth curve passing through the observed h(x) values. The surfaces $F_1(x,y) = g(x)$ and $F_2(x,y) = g(x) + cy^2$, with a suitable non-negative constant c on a bounded domain, coincide on y = 0. They consequently predict identical values along the measured line while differing away from it. This is a mathematical argument about missing transverse observations. No two-dimensional interpolation, surface reconstruction, or artificial experimental image is generated from the archive.

The calculations used Python 3.12.14 and NumPy 2.3.5. Numerical outputs were checked against the stated formulas and published inputs. No confidence intervals are assigned because the purpose is an exact constructive demonstration, and a complete acquisition uncertainty model was not recovered for the spatial table. No new diffraction experiment, coherent reconstruction, spatial calibration, or independent defect measurement was performed. The same original measurements may support other secondary treatments; the present contribution concerns the information required for mapping and the non-uniqueness of height-based interpretation.

A modern uncertainty analysis would first distinguish counting statistics, fitting uncertainty, angular-zero and scale calibration, illumination variability, background subtraction, spatial positioning, and temporal drift. For independent positive rate estimates K and R, with the ratio defined as h = K/R, an illustrative first-order uncertainty propagation is given by:

$$\left(\frac{u_h}{h}\right)^2 \approx \left(\frac{u_K}{K}\right)^2 + \left(\frac{u_R}{R}\right)^2$$

When the estimates K and R, are correlated, the expression becomes:

$$\left(\frac{u_h}{h}\right)^2 \approx \left(\frac{u_K}{K}\right)^2 + \left(\frac{u_R}{R}\right)^2 - \frac{2\,cov(K,R)}{KR}$$

Where u_h, u_k, and u_r denote the standard uncertainties of h, K, and R, respectively, and cov(K,R) represents the covariance between the two rate estimates. These expressions are offered as a prospective uncertainty-analysis procedure rather than as estimates for the historical measurements. The tabulated rates alone do not establish observation times, statistical independence, counting distributions, or systematic uncertainties. Consequently, no numerical uncertainties have been artificially assigned to the measurements reported in Table 1.

4. Results

The synthesis identifies a progression in retained information that is more precise than classifying measurements by whether their output resembles an image. A selected height at each position records one descriptor of an angular response. A full profile at each position retains shape and permits several descriptors to be examined together. A two-dimensional spatial grid adds transverse information. Additional reciprocal-space directions or reflections add constraints on the structural interpretation. Fig 1 illustrates the historical measurement geometry and a proposed extension that preserves spatially registered angular scans.

The evidence classes used throughout the analysis are: (A) directly retained measured quantities, such as the tabulated rates and nominal positions; (B) deterministic transformations of those quantities, such as $\frac{K}{R}$ and $\frac{V}{R}$; (C) constructed examples that are compatible with the retained summaries but not fitted to measured profiles; and (D) unknown historical characteristics, including actual profile widths, integrated angular areas, component-specific spatial response and transverse variation. Keeping these classes separate prevents a visually plausible illustration from being mistaken for a recovered observation.

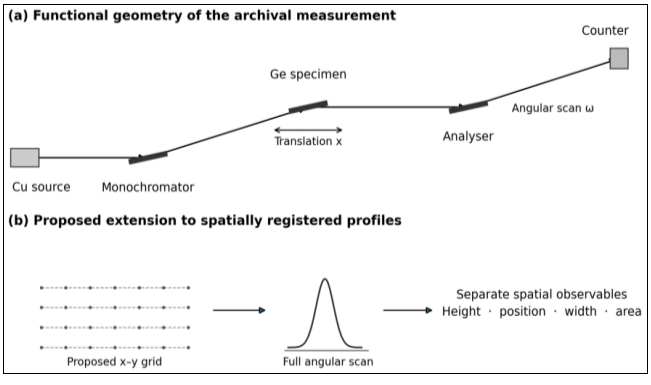

Fig 1: Functional measurement geometry and a proposed extension for mapping

Note: Original schematic based on the triple-crystal geometry described by [3]. Optical paths are functional, not to scale. Panel (b) shows a proposed acquisition design; its raster and profile are schematic and do not represent a measured surface or recovered scan. The archived spatial record contains one line of selected peak heights.

The archived series establishes differential spatial contrast under its reported conditions. Table 1 reproduces all eleven rates and the calculated peak-height ratios. K/R ranges from 0.07313 at 20 mm to 0.34110 at 0 mm, a maximum-to-minimum factor of 4.664. V/R ranges from 0.22615 to 0.25074, a factor of 1.109. These are descriptions of the reported maxima. The comparatively stable dynamical ratio helps identify a differential component response, but it does not demonstrate equal spatial kernels or prove that normalization removes every boundary effect.

Table 1: Archived Ge 111 spatial rates and calculated peak-height ratios

x (mm)	K (s^{-1})	R (s^{-1})	V (s^{-1})	K/R	V/R
0	177.2	519.5	121.0	0.34110	0.23292
2	266.7	825.1	186.6	0.32323	0.22615
4	196.9	845.6	196.6	0.23285	0.23250
6	162.1	806.4	197.4	0.20102	0.24479
8	136.2	813.4	190.3	0.16745	0.23396
10	145.3	846.0	201.5	0.17175	0.23818
12	161.0	882.8	216.6	0.18237	0.24536
14	139.0	810.0	203.1	0.17160	0.25074
16	100.1	770.1	188.7	0.12998	0.24503
18	63.6	623.4	153.4	0.10202	0.24607
20	29.5	403.4	92.4	0.07313	0.22905

Note: Source rates are from [3, Table VII, printed p. 200; PDF p. 211]. The reported detuning is 70 arcsec. K is the additional component; R and V are residual and virtual dynamical components. Ratios are calculated from the published rates. Reported decimal precision is not a complete measurement-uncertainty statement.

The constructive example exposes the additional information required for an area map. For the fixed-width family, the integrated normalized intensity changes from 7.262 arcsec at 0 mm to 1.557 arcsec at 20 mm. It follows the spatial variation in height. For the variable-width family, the area is 3.656 arcsec at every position, including both endpoints. The necessary illustrative widths range from 10.07 to 46.97 arcsec. Both families reproduce every h(x) exactly. Selected values are shown in Table 2, and Fig 2 compares representative angular profiles and the resulting area descriptions.

Table 2: Two hypothetical profile families compatible with selected source maxima

x (mm)	h = K/R	Fixed width (arcsec)	Variable width (arcsec)	Fixed-width area (arcsec)	Variable-width area (arcsec)
0	0.34110	20.00	10.07	7.262	3.656
2	0.32323	20.00	10.63	6.881	3.656
8	0.16745	20.00	20.51	3.565	3.656
10	0.17175	20.00	20.00	3.656	3.656
20	0.07313	20.00	46.97	1.557	3.656

Note: Only h is derived from the observations. Every width and area in this table is constructed, not measured. Both families reproduce all eleven source heights; five representative positions are displayed. The variable-width family has constant area analytically. Calculations use unrounded ratios.

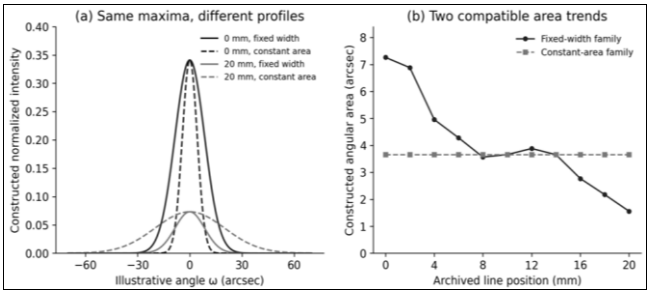

Fig 2: Constructive demonstration that the retained maxima do not determine angular areas

Note: All curves and areas are hypothetical mathematical constructions using h = K/R from Table 1. Panel (a) shows two endpoint examples; panel (b) uses all eleven source heights. The fixed width is 20 arcsec. The other family uses $w_2(x) = 20h(10\ mm)/h(x)$. Centres, widths, and areas are not experimental determinations. Areas are integrals of dimensionless illustrative profiles over angle, not absolute cross sections.

The ratio between the largest and smallest heights is therefore consistent with the same ratio between areas in one family and with no area variation in the other. This result is an information argument rather than a newly observed redistribution of scattering. The hypothetical widths cannot be used to claim that broadening explains the archival series. Conversely, the maxima alone cannot establish that broadening is negligible. Full profiles or independently justified width constraints would be needed to distinguish these possibilities for the original specimen.

An important robustness implication follows from the general scale-family result in the Theoretical Background: The conclusion survives replacing the Gaussian with any suitable normalized shape whose area changes with its scale parameter. However, stronger physical claims would require testing the same height-only ambiguity in dynamical-diffraction simulations that include the monochromator, analyser, sample response and scan window. Such a simulation would be a prospective extension; it is not presented as completed evidence in the present article.

The distinction remains after improving spatial sampling. Measuring many more maxima along the same line would give a more densely sampled height profile while preserving the height–width ambiguity. Likewise, smoothly interpolating the eleven heights would not determine an unsampled transverse direction. The surfaces F_1 and F_2 defined in the method agree at every measured location and differ for $y \neq 0$. A coloured two-dimensional display based only on the line would consequently depict an added assumption about transverse structure. It would not constitute a measured two-dimensional diffraction map.

The literature comparison identifies which additional observations address these limitations. Table 3 summarizes the methods by their data and interpretation. Rocking-curve imaging directly addresses loss of local angular shape by recording an image sequence during angular scanning. [5] Demonstrate this approach for diamond and silicon optics. [6] Analyse local rocking curves in a 4H-SiC epilayer using cumulative integrated intensity and extract descriptors useful for complex profiles. Their work supports retaining and analysing the profile rather than assuming that one fitted maximum represents all available information. It does not

establish that every profile can be assigned a unique defect mechanism.

Reciprocal-space mapping addresses a different limitation by resolving intensity along more than one scattering coordinate. [4] Explains its advantages over a single scan for separating features in the measured diffraction distribution. Such maps can help distinguish radial and transverse changes under a suitable geometry, but a reciprocal-space map is not itself a real-space image. Combining it with specimen translation adds spatial localization while increasing demands on acquisition, registration, and response characterization.

Spatially resolved measurements also require geometric corrections even when many angular images are available. [17] Show that a monochromator–sample Bragg-angle mismatch affects rocking-curve imaging of an ammonium dihydrogen phosphate crystal, including the image dimensions relevant to a dispersion correction. This is a different specimen and geometry from the Ge archive. Its methodological relevance is that detector positions, angular positions, and specimen coordinates need a calibrated transformation before local curvature or profile shifts are assigned to the crystal.

Scanning microdiffraction, dark-field microscopy, and coherent imaging provide further constraints through different measurement operators. [7] Demonstrate orientation and strain/stress mapping in metal thin films using localized diffraction. [8] Demonstrate dark-field microscopy for internal crystalline structures in aluminium. [10] Reconstruct a deformation-related phase in a lead nanocrystal from coherent diffraction. These studies establish distinct measurement principles; their reported capabilities cannot simply be transferred to a bulk Ge specimen measured with a conventional triple-crystal arrangement.

Direct semiconductor examples reinforce the role of the measurement model. [9] Compare scanning diffraction and Bragg projection ptychography in a heterostructured GaInP/InP nanowire, relating spatial resolution to the quantitative interpretation of strain. The comparison shows that a strain map depends on how the measurement resolves the relevant structure. [18], in crystalline oxide thin films, use grazing-incidence diffuse scattering with broad reciprocal-space coverage to investigate local order. Their method provides a different kind of structural information and should not be described as a spatial defect-density image of the historical Ge surface.

Table 3: Information supplied by distinct diffraction measurement approaches

Approach	Data retained	Derived information and principal condition
Selected heights along a line	One or several peak maxima at each position.	Differential contrast along the sampled line; areas and transverse structure remain undetermined.
Rocking-curve imaging	Registered spatial images over an angular scan.	Local profile descriptors, with angular and spatial calibration and adequate coverage [6, 5].
Reciprocal-space mapping	Intensity over defined scattering-vector coordinates.	Separation of reciprocal-space features under a geometrical model; real-space location requires further localization [4].
Scanning microdiffraction	Diffraction distributions at localized probe positions.	Orientation and strain-related constraints with indexing, spatial-response and geometrical models [7].
Dark-field X-ray microscopy	Diffracted-beam images with optical and angular selection.	Internal spatial structure with resolution and acceptance defined by the imaging configuration [8].
Coherent Bragg imaging or ptychography	Coherent reciprocal-space data, with overlap for ptychography.	Reconstructed complex object and displacement projections subject to coherence, sampling, and reconstruction assumptions [9, 10].

Note: The entries describe measurement principles, not equivalent performance specifications. Cited demonstrations concern different specimens and geometries. No resolution ranking or universal structural identification is implied.

The synthesis yields a measurement strategy expressed in Table 4. For a claim about angularly integrated selected-channel contrast, a complete profile, a defined integration interval, background treatment, and flux information are needed. For a claim about position or width, angular registration and instrumental response are necessary. A real-space map additionally requires spatial coverage and a justified spatial response. Structural assignment requires further constraints appropriate to the mechanism. These requirements are conditional on the intended claim; they do not prescribe a single universally optimal instrument.

The proposed framework can be implemented as a sequence of seven linked decisions. First, state the measurand and its units (for example, maximum count rate, integrated profile area, angular displacement or a model-derived strain component). Second, identify the raw dimensions of intensity data retained at each coordinate, including whether maxima were tracked or a fixed angle was sampled. Third, specify the angular or reciprocal-space coverage and test whether shifted, split or overlapping profiles fall inside it. Fourth, characterize spatial support and registration, not merely translation increments or detector pixels. Fifth, calibrate instrumental response, illumination and drift and propagate appropriate uncertainties. Sixth, formulate competing physical interpretations and identify the extra reflections, independent modalities or mechanistic models that distinguish them. Seventh, report the resulting map under the strongest label justified by those observations, explicitly separating an operational contrast map from a quantitative structural map. These decisions constitute a proposed audit trail for map interpretation, not an empirically benchmarked decision instrument.

Table 4: Proposed measurements linked to the intended mapping claim

Intended claim	Additional evidence required	Ambiguity addressed
Selected-channel angular area varies spatially.	Profiles over a justified interval; background, overlap, and flux treatment.	Height variation caused by width changes or incomplete angular coverage.
Local angular position or width changes.	Registered angular coordinates and an instrument-response model or calibration.	Apparatus contributions and angular-zero differences.
A two-dimensional contrast distribution is measured.	Spatial coverage in both directions and an estimated spatial response.	Unobserved transverse variation and footprint averaging.
Contrast represents strain rather than rotation.	Appropriate reciprocal-space directions, additional reflections, and a justified deformation model.	Mixing of lattice-spacing and orientation effects.
Contrast quantifies a particular defect population.	A mechanism-specific scattering model and independent structural constraints or calibration.	Non-unique sensitivity to termination, roughness, strain, and disorder.
A pattern is stable across acquisition.	Repeated reference visits, monitored throughput, and acquisition-order checks.	Temporal drift or positioning history masquerading as spatial contrast.

Note: This is a proposed measurement strategy, not a completed experimental protocol or a validated decision instrument. Requirements should be adapted to the actual specimen, geometry, and measurand.

A practical extension of the historical experiment would begin by recording full analyser scans at selected specimen locations while monitoring incident intensity. Repeated visits to reference locations and reversing the scan order would help distinguish specimen variation from drift and positioning history. A measured footprint and appropriate edge measurements would constrain spatial averaging. Only after those observations were characterized would a raster scan provide a defensible basis for displaying height, position, width, and area as separate spatial observables. None of these proposed measurements is reported as having been performed here.

Table 5: Evidence-status classification for the archival reanalysis

Evidence class	Example in this article	Permissible claim
A. Measured	K, R and V peak rates at eleven listed positions	Observed component-specific spatial contrast
B. Derived	K/R and V/R from the reported rates	Relative peak-height comparison, not calibrated defect density
C. Constructed	Gaussian profiles, their widths and angular areas	Non-uniqueness of recovery from the retained maxima
D. Unknown	Raw historical full profiles, transverse map, response kernels	No retrospective recovery or structural inversion

A focused validation study could apply the procedure to an independently acquired, spatially registered diffraction stack for which full curves, reference measurements and footprint estimates are retained. Peak height, centroid or fitted peak position, width and angular area could then be mapped on the same specimen coordinates; disagreements would be assessed against angular-window truncation, drift and response calibration. Replication at a second non-equivalent reflection or comparison with independent surface characterization would specifically test competing strain, tilt and disorder assignments. The present article proposes these tests without assigning performance improvements or invented validation outcomes.

5. Discussion

The main result is that the transition from selected peak heights to quantitative maps requires additional constraints in both angular and real space. The archived observations support a spatially varying selected-component response. They do not uniquely specify the corresponding integrated angular signal or the unmeasured transverse distribution. The constructive examples make this limitation explicit without requiring a disputed microscopic explanation of the historical peak.

The added value of the framework lies in matching each proposed inference with its evidentiary prerequisites. A map labelled ‘K/R peak-height ratio’ can be valid as a record of conditional contrast despite incomplete physical identification; a map labelled ‘integrated scattering’, ‘strain’ or ‘defect density’ demands progressively stronger acquisition, calibration and model assumptions. This graduated terminology is relevant to both archival reanalysis and contemporary multimodal diffraction, where visually dense datasets can conceal underdetermined inverse steps.

This contribution differs from a further comparison of normalization choices or coefficients of variation. Those comparisons describe the robustness and magnitude of the observed contrast. The present question concerns the information lost when angular profiles are compressed and the evidence needed when that contrast is promoted to a structural map. The mathematical non-uniqueness is elementary, but its application clarifies which follow-up measurement would address a particular ambiguity. The framework is a synthesis of established measurement principles rather than a new imaging technique.

The distinction between maxima and fixed-angle intensity is especially consequential. A strong spatial feature in a fixed-angle image may arise because the local profile moves through the accepted angular window. Tracking the local maximum can remove that particular contrast mechanism while retaining sensitivity to width and amplitude. Integrating a sufficiently complete profile addresses another aspect but still requires careful background subtraction and an appropriate measurement model. No single descriptor can be assumed to be a universally more faithful map of defects.

Integrated intensity also has limits. It depends on the interval, overlap treatment, polarization and absorption conditions, and acceptance of the instrument. The Gaussian areas in this article are integrals of hypothetical normalized angular profiles, not absolute scattering cross sections. An experimental area map would require documenting the actual scan coordinate and any conversion to reciprocal space. Strong dynamical effects can make a simple interpretation in terms of independent scattering centres inappropriate. The relevant physical model must match both the specimen and the optical arrangement.

Surface sensitivity and depth specificity should likewise be distinguished. The historical treatment experiments and topographic proposal motivate attention to the surface

region [1]. They do not assign a calibrated penetration-depth distribution to each spatial observation. Surface termination, roughness, strain, and lattice disorder may modify intensity in overlapping regions of reciprocal space. The theories of [14], [15], and [16] address different conditions within this broad problem. Choosing between such mechanisms requires evidence beyond a contrast image.

A spatially dense measurement can still be weakly constrained structurally. Detector pixel size, scan step, beam footprint, reconstructed voxel size, and demonstrated resolution describe different properties. Fine pixels can oversample a blurred response; a fine translation grid can oversample a broad footprint. Conversely, coarse sampling can conceal variation that an adequately localized probe could resolve. The 2 mm spacing in the archived line therefore cannot establish either a 2 mm resolving power or the smallest defect structure present in the specimen.

The different mapping methods should be selected by the unresolved physical question. Rocking-curve imaging is suitable when local angular shape and orientation contrast are central. Reciprocal-space mapping is useful when scattering features overlap in a single angular trace. Localized diffraction adds real-space selectivity, while dark-field microscopy selects diffracting internal volumes. Coherent Bragg methods use phase-sensitive reconstruction under their own data and modelling conditions. These distinctions follow the literature comparison; they do not imply that each method independently returns a complete strain tensor or a unique defect inventory.

The techniques also have different failure modes. Rocking-curve imaging preserves local angular dependence but remains susceptible to angular misregistration, response broadening and peak overlap. Reciprocal-space mapping can separate scattering directions but does not automatically localize them within a specimen. Scanning microdiffraction adds spatial selection at the cost of footprint and positioning constraints. Dark-field microscopy involves optical and angular acceptance that must be reflected in the reconstructed spatial support. Coherent Bragg approaches introduce phase-retrieval, coherence and reconstruction assumptions; a single reflection typically measures a projected displacement rather than an unrestricted three-dimensional vector field. None of these methods by itself converts intensity contrast into a unique microscopic defect inventory.

For coherent Bragg imaging, the reconstructed phase is related to a projection $G \cdot u$ of the displacement field, up to the Fourier sign convention and relevant phase ambiguities. One reflection does not automatically provide the full vector displacement. Combining non-coplanar reflections can add independent projections but requires consistent registration and sufficient reconstruction quality. [9] Also illustrate the importance of matching the spatial response to the structure being interpreted. The additional mathematical sophistication of a reconstruction increases the need to specify what is measured and what is inferred.

The proposed acquisition strategy separates economical reconnaissance from quantitative mapping. A limited number of complete profiles can reveal whether peak motion, splitting, or broadening makes a height-only image difficult to interpret. That information can guide angular windows and the spatial region selected for a more extensive scan. Repeating reference measurements provides a check on time-dependent changes that otherwise become confounded with position. This strategy is proposed because each step addresses a specific ambiguity identified by the synthesis. Its efficiency and reliability have not been experimentally evaluated in this study.

The archival record also places limits on retrospective conclusions. The original spatial measurements were not acquired as a modern multidimensional image stack, and complete raw profiles and response calibrations were not recovered for this reanalysis. Their absence from the examined materials does not establish that the original experiment was deficient for its stated purpose. It limits new questions that require those inputs. [19] Discuss the value of retaining raw diffraction records for subsequent scrutiny and reuse; preserving selected maxima alone narrows the range of future analyses.

Several limitations apply to the present synthesis. The literature selection is purposive and includes different material classes and instrumental geometries. The archival example concerns one specimen and one line, so it cannot estimate the prevalence of a particular ambiguity across semiconductor characterization. The Gaussian families establish non-uniqueness for the specified summary representation but do not exhaust physically plausible profiles or reproduce coherent dynamical wavefields. The line-to-surface construction is similarly a demonstration of missing information, not a model of the specimen surface. These distinctions prevent the illustrations from being interpreted as recovered experimental results.

The proposed procedure has not been evaluated for sensitivity, specificity, acquisition efficiency or inter-analyst reproducibility. Its claim-evidence links synthesize established physical constraints, while their organization into a decision workflow is methodological interpretation. Consequently, the contribution should be judged as an auditable conceptual framework and constructive counterexample, not as proof that following the workflow improves instrument performance. Material-dependent dynamical constraints could narrow the admissible profile families but cannot be inferred retroactively from selected maxima.

Future evaluation should test the proposed distinctions on spatially registered raw datasets with known acquisition conditions. One useful comparison would extract height, centroid or maximum position, width, and area maps from the same profile stack and examine where they agree or differ. Controlled changes in orientation or instrumental response could test whether a feature assigned to the specimen persists after the relevant correction. Independent surface characterization and measurements at additional reflections would help assess structural assignments. Such studies would evaluate the practical value of the proposed strategy rather than merely reproduce its analytical counterexamples.

The article also offers a useful setting for teaching scientific measurement. Students can examine how two profiles share the same maximum but imply different areas, or why a line cannot determine a surface. The difficulty lies in identifying the extra assumption required for the inference, rather than in performing the arithmetic alone. This is a potential educational application; no student data or learning outcomes are reported. Its relevance follows from the same distinction between an observable and a structural

interpretation that governs the scientific analysis.

6. Conclusion

Selected diffraction peak heights can reveal spatial contrast while leaving substantial ambiguity about angular redistribution and structural origin. In the archival Ge(111) series, the additional-to-reference peak ratio varies strongly across the sampled line. The same retained maxima nevertheless admit mathematical profile families with different area trends, and the line supplies no unique transverse map. These results establish limits on the information recoverable from the summaries; they do not identify the actual missing profiles.

A defensible transition to spatial diffraction maps requires defining the measurand, retaining the angular information relevant to it, characterizing the spatial and instrumental response, and collecting additional structural constraints where necessary. The synthesis of established and recent methods provides a basis for selecting those measurements. It supports reporting measured contrast maps precisely and reserves stronger labels, such as strain or defect-density maps, for interpretations supported by the required evidence. The practical contribution is a seven-decision audit of measurement claims: Define the observable, preserve appropriate raw dimensions, check angular coverage, establish spatial response, calibrate the instrument, test alternative structural models and label each map according to the evidence actually available. The framework retains the value of the 1986 Ge(111) measurements as documented spatial contrast while marking the boundary between those historical observations and quantities that would require new measurement. Its effectiveness remains a subject for prospective tests on complete spatially registered diffraction data.

7. Author's Note

On the occasion of my retirement, following four decades of academic service, I have returned to the experimental research undertaken during my doctoral studies in the 1980s. This article forms part of a retrospective reassessment of that work in light of subsequent theoretical and methodological developments. Its purpose is to examine the continuing scientific value of the archived observations, clarify their limitations, and identify questions that remain unresolved. The original thesis and related publications are explicitly acknowledged, and the historical measurements are distinguished from the analyses undertaken for the present article.

8. References

1. Alexandropoulos NG, Kotsis KT. Use of kinematical diffraction in X-ray topography. J Appl Crystallogr. 1985; 18(6):513-518. Doi: 10.1107/S0021889885010809
2. Kotsis KT, Alexandropoulos NG. Diffraction pattern near the Bragg angle for an asymmetrically cut crystal. J Appl Crystallogr. 1986; 19(6):473-476. Doi: 10.1107/S0021889886088921
3. Kotsis KT. Dynamiki kai kinimatiki skedasi ton aktinon-X konta se simeio tou antistrofou plegmatos [Dynamical and kinematical X-ray scattering near a reciprocal-lattice point] [doctoral dissertation]. Ioannina: University of Ioannina, 1986. Doi: 10.12681/eadd/0880
4. Fewster PF. Reciprocal space mapping. Crit Rev Solid State Mater Sci. 1997; 22(2):69-110. Doi: 10.1080/10408439708241259
5. Halavanau A, Margraf R, Robles R, MacArthur J, Qu Z, Marcus G, *et al*. Experimental setup for high-resolution characterization of crystal optics for coherent X-ray beam applications. J Appl Crystallogr. 2023; 56(1):155-159. Doi: 10.1107/S1600576722010998
6. Estiri A, Bytheway R, Lafford TA, Fox OJL, Graham A, Hurley C, *et al*. A novel approach for analysis of rocking curve X-ray diffraction imaging data (RC-XRDI) on 4H-SiC using cumulative integrated intensity (CII) method. J Electron Mater. 2025; 54(7):5075-5086. Doi: 10.1007/s11664-025-11963-y
7. Tamura N, MacDowell AA, Spolenak R, Valek BC, Bravman JC, Brown WL, *et al*. Scanning X-ray microdiffraction with submicrometer white beam for strain/stress and orientation mapping in thin films. J Synchrotron Radiat. 2003; 10(2):137-143. Doi: 10.1107/S0909049502021362
8. Simons H, King A, Ludwig W, Detlefs C, Pantleon W, Schmidt S, *et al*. Dark-field X-ray microscopy for multiscale structural characterization. Nat Commun. 2015; 6:6098. Doi: 10.1038/ncomms7098
9. Hammarberg S, Dzhigaev D, Marçal LAB, Dagytė V, Björling A, Borgström MT, *et al*. Fast nanoscale imaging of strain in a multi-segment heterostructured nanowire with 2D Bragg ptychography. J Appl Crystallogr. 2024; 57(1):60-70. Doi: 10.1107/S1600576723010403
10. Pfeifer MA, Williams GJ, Vartanyants IA, Harder R, Robinson IK. Three-dimensional mapping of a deformation field inside a nanocrystal. Nature. 2006; 442(7098):63-66. Doi: 10.1038/nature04867
11. Batterman BW, Cole H. Dynamical diffraction of X rays by perfect crystals. Rev Mod Phys. 1964; 36(3):681-717. Doi: 10.1103/RevModPhys.36.681
12. Lucas CA, Gartstein E, Cowley RA. The resolution function of an X-ray triple-crystal diffractometer: Comparison of experiment and theory. Acta Crystallogr A. 1989; 45(6):416-422. Doi: 10.1107/S010876738900108X
13. Guigay JP, Sanchez del Rio M. Formulation of perfect-crystal diffraction from Takagi–Taupin equations: Numerical implementation in the crystalpy library. J Synchrotron Radiat. 2024; 31(6):1469-1480. Doi: 10.1107/S160057752400924X
14. Robinson IK. Crystal truncation rods and surface roughness. Phys Rev B. 1986; 33(6):3830-3836. Doi: 10.1103/PhysRevB.33.3830
15. Sinha SK, Sirota EB, Garoff S, Stanley HB. X-ray and neutron scattering from rough surfaces. Phys Rev B. 1988; 38(4):2297-2311. Doi: 10.1103/PhysRevB.38.2297
16. Karpov AV, Kazakov DV, Punegov VI. Dynamical theory of X-ray diffraction by crystals with different surface relief profiles. Acta Crystallogr A Found Adv. 2023; 79(2):171-179. Doi: 10.1107/S2053273322012062
17. Ferrari E, Ferrari C, Baruchel J, Caliste TNT, Basso S, Chauhan A, *et al*. Compensation of chromatic dispersion in rocking curve imaging for high-resolution X-ray diffraction profile measurements. J Appl Crystallogr. 2026; 59(1):130-134. Doi:

10.1107/S1600576725010349
18. Bang J, Strkalj N, Sarott MF, Kholina Y, Trassin M, Weber T. High-energy diffuse X-ray scattering at ultra-small-angle grazing incidence for local structure study of single-crystalline thin films. J Appl Crystallogr. 2025; 58(4):1417-1427. Doi: 10.1107/S1600576725005837
19. Kroon-Batenburg LMJ, Lightfoot MP, Johnson NT, Helliwell JR. Raw diffraction data and reproducibility. Struct Dyn. 2024; 11(1):011301. Doi: 10.1063/4.0000232